Trajectory adaptation of biomimetic equilibrium point for stable locomotion of a large-size hexapod robot

Trajectory Adaptation of Biomimetic Equilibrium Point for Stable Locomotion of a Large-size Hexapod Robot

Chen Chen[1] · Fusheng Zha[1] · Wei Guo[1,*] · Zhibin Li[2,*] · Lining Sun[1] ·
Junyi Shi[1]

Abstract This paper proposes a control scheme inspired by the biological equilibrium point hypothesis (EPH) to enhance the motion stability of large-size legged robots. To achieve stable walking performances of a large-size hexapod robot on different outdoor terrains, we established a compliant-leg model and developed an approach for adapting the trajectory of the equilibrium point via contact force optimization. The compliant-leg model represents well the physical property between motion state of the robot legs and the contact forces. The adaptation approach modifies the trajectory of the equilibrium point from the force equilibrium of the system, and deformation counteraction. Several real field experiments of a large-size hexapod robot walking on different terrains were carried out to validate the effectiveness and feasibility of the control scheme, which demonstrated that the biologically inspired EPH can be applied to design a simple linear controller for a large-size, heavy-duty hexapod robot to improve the stability and adaptability of the motion in unknown outdoor environments.

Wei Guo
Harbin Institute of Technology, No.92 West Dazhi Street, Harbin, Heilongjiang Province, China
E-mail: wguo01@hit.edu.cn

Zhibin Li
School of Informatics, the University of Edinburgh
E-mail: zhibin.li@ed.ac.uk

1 Introduction

On discontinuous terrain surfaces, legged robots can achieve significant mobility advantages in such a challenging environment compared to wheeled types [1, 2]. But by far, legged robots are still not as agile as legged animals on this planet. Stable and robust motion control of different kinds of legged robots, especially large-size legged robots, remains an important research topic to address [3–6]. Particularly for a large-size legged robot, the deformations of robot structure, ie body and legs, as well as the significant foot-ground impacts are not negligible and can largely downgrade the walking performance, ie motion stability and body attitude, especially on tough terrains. Compared to small-size legged robots, large-size robots have difficulty in recovering the body posture due to very large inertia, and the resulted instability may further lead to irreversible damage to the robot. Therefore, the capability of enhancing a stable motion is of crucial importance for large-size legged robots.

The core of stable motion control of legged robots is how to control the motions of the legs properly [7]. This is hard because of the mechanical complexity, redundant degrees of freedom, unknown terramechanics, and so on. But even though the biomechanical properties of limbs are complex, a wide variety of activities can still be taken by the legged creatures without much knowledge known beforehand about the environments. Inspired by the motion dexterity of legged creatures, and motivated by the understanding and further applications of the biological motion mechanisms, many proposals have been presented by the neuroscientists through long term observations and experiments on different species. Among all the proposals, mechanical

reductionism and equilibrium point hypothesis may be most directly related to the legged robot control.

In the field of mechanical reductionism, scholars believe an assumption that motor actions of limbs can be reduced to mechanical programming. In line with this assumption, they argue that the central nervous system (CNS) forms internal models of limbs, namely the inverse dynamics models [8–12]. The EMG activities and torques underlying the control process of limbs are in continuously programming and computing by the CNS using the inverse dynamics models. Based on the mechanical reductionism, many controllers using inverse dynamics have been developed for bionic limb controlling. Villard et al. [13] designed a controller based on the inverse dynamics model of the quadruped robot RALPHY to achieve stable locomotion. In their controller, the inverse dynamics model was used for the single leg control level to get the joint torque needed. Li et al. [14] proposed a controller based on a constrained dynamics model for a quadruped robot with flexible joints. In this controller, a dynamic force distribution approach and a fuzzy-based adaptive control method of the joints were proposed to suppress uncertainties of the perturbing forces and the dynamics model. Roy et al. [15] proposed an energy efficient controller for the hexapod locomotion based on the analysis of the dynamics model of a hexapod robot. The energy consumption model was established based on the dynamics model. The effectiveness of the controller was verified through simulation experiments. A similar idea of energy consumption optimization based on the inverse dynamics model was also employed by Mahapatra et al. [16] in designing their controller for the hexapod locomotion. To realize better dynamic quadrupedal locomotion of a robot called StarlETH, Hutter et al. [17] proposed an operational space controller based on hierarchical task optimization. The projected dynamics model of floating base systems was used to reduce the optimization dimensionality.

Although the inverse dynamics model is widely employed by scholars in designing their controllers, but it may not be the ultimate key to solve the robot motion control problem. At least two limitations need to be further breached. The first is the complexity of modeling. Modern robots are developing rapidly. New structures, like legged robots with flexible joints, and redundant mechanical degrees of freedom (DOFs) severely challenge the dynamics modeling process. The second is the model accuracy. A dynamic motion process usually shows strong nonlinear characteristics. For a robot motion controller based on dynamics modeling, model parameters may be time-varying and need to be estimated with high accuracy to get a good control performance [18–21]. But the reality is that some unpredictable quantities, like joint frictions or the disturbances from the environment, are hard to be estimated. Therefore additional compensations for model uncertainties [22, 23], or interactive models with environments [24] are always needed. The two limitations together lead to a great amount of nonlinear computations. The expensive computations are not friendly with the designing of real-time controllers. Besides, whether the CNS needs to know the exact model of the musculoskeletal system is still a debatable question, because the control process seems to be quite time-consuming and difficult for a biological system.

In contrast to the inverse dynamics control, the equilibrium point hypothesis (EPH) pioneered by Feldman [25] seems more in line with biological motions. Triggered by the observations of human motor behaviors, Feldman did systematically theoretical and experimental efforts, and proposed that the limb motion was controlled in the way of shifting the limb from one equilibrium position to another. In other words, motor control could be realized by adjusting a succession of equilibrium points (EPs) overtime [26]. He proposed a model to describe the function of the muscle-reflex system. In this model, the muscle was abstracted into a spring with adjustable resting length. Therefore, muscle force only related to the spring stiffness, and the difference between the actual length/position and the equilibrium length/position [27]. During the EP transition process, no knowledge about the environment or the internal model of the musculoskeletal system is needed. The functional tuning of the CNS remains constant. This hypothesis has been putting forward by many scholars for its compelling feature that motion and posture are integrated into a single mechanism [28–32]. Obviously, compared with the inverse dynamics control, the EPH can avoid the uncertain parameters and complex nonlinear computations. Therefore, it is more attractive when an effective real-time controller is needed in real-world deployment.

Regardless of the various hypotheses of EPH for motor control in biological systems [33–35], many EP controllers have been developed and implemented on different robots successfully due to the original tolerance for the unpredicted external disturbances. Taking advantages of the muscle-spring model, Gu et al. [36] developed a two-phase EP controller for controlling simulated human movements. In this controller, given a task in Cartesian space, the EP solutions were computed in joint space based on the idea of minimizing gravity potential energy. Motion executions were taken charged by the muscle-spring model. According to EPH, the force exerted on a limb depends on the difference between the actual positions and EPs, and the stiffness

and damping parameters about the EPs. Based on this, Mukaibo et al. [37] developed a two-linked manipulator with a double-actuator joint to generate human-like movements. One of the actuators was used for position control, and the other was used for the joint stiffness control. Using a simple control scheme, this mechanism could allow a robot limb to achieve self-stability in unknown environments. A similar idea inspired by the EPH was also employed by Kim et al. [38] and Park [39] in designing their redundant actuation manipulators. Jain et al. [40] proposed a control scheme based on the EPH for a 7 DoF anthropomorphic arm with series elastic joint actuators. In this control scheme, two controllers to generate the Cartesian space EPs for the arms end effector were developed. Then using the inverse kinematics, the joint EPs could be obtained. Geng et al. [41] developed a control structure for a planar biped walking robot. In this control structure, a local joint EP controller was designed to realize the control of a single joint. Stable walking was achieved without any computation of the robot dynamics. Shi et al. [42] proposed an EP controller for a quadruped robot. In this controller, by solving a QP problem to achieve desired equilibrium contact forces, the foot-tip EPs were indirectly obtained. The effectiveness of the controller was verified through a series of experiments.

Because the EPH was originated from the studies of humans, so the applicability of EP controllers for controlling limb-like manipulators is very desirable [43]. Nevertheless, although controllers inspired by the EPH show significant advantages in many aspects, EP controllers designed for legged robots, especially for large-size legged robots, are rarely seen. Legged robots are base-floating systems with redundant DoFs. Both single-leg control and inter-leg coordination should be taken into account when a good controller is wanted to be designed. Furthermore, unlike manipulators that operate in unchanged specific environments, legged systems usually work in unstructured environments. The complex interaction between the feet and terrains will significantly affect the motion states of the robots. Therefore, how to obtain stable EP trajectories is the main problem currently limiting the development of EP controllers for legged systems.

Inspired by the advantages of the currently developed EP controllers, and motivated by solving the stable walking problem of a large-size hexapod robot, a simple control scheme based on an EP trajectory modification method is proposed in this paper. Based on the compliant-leg model established in this control scheme, no nonlinear dynamics computations are employed when designing the whole control logic. The whole control scheme is totally linear, and easy to be realized. An EP trajectory modification method is introduced in the control scheme. Different from the existing stable control methods for small legged robots, the deformations of the large-size hexapod robot which cannot be ignored are significantly considered while designing the EP trajectory modification method. Through the work of the control scheme, stable hexapod locomotions can be realized just by adjusting the EP trajectories over time without any knowledge about the environment. Therefore good versatility of the control scheme can be ensured.

This paper is organized as follows: in the second part, the control problems of the large-size hexapod robot and the control scheme are introduced briefly. In the third part, an EP trajectory modification method via contact-force optimization is introduced in detail. In the fourth part, the experiment results to demonstrate the effectiveness of the control scheme are discussed.

2 The hexapod robot system and the control scheme inspired by EPH

2.1 The problem statement of the large-size hexapod robot

The large-size hexapod robot developed for large load carrying transportation in challenging outdoor environments is depicted in Figure 1. The robot is designed in the size of over 4 m×2.5 m×2 m while the weight of it is 2.5 t. The left three legs are marked as leg 1, leg 2 and leg 3 while the right three legs are marked as leg 4, leg 5 and leg 6. Three electrically actuated joints are assembled on each leg of the robot, which are the horizontal joint (H-joint), the vertical joint (V-joint), and the swing joint (S-joint). Various sensors, such as an inertial measurement unit (IMU), 3D contact-force sensors, joint-displacement sensors, are equipped on this robot. The IMU is used to obtain the robot body attitude values during walking (the attitude angles, attitude angular velocities and attitude angular accelerations). The 3D contact-force sensor equipped on each foot of the robot is used to detect the contact forces of each leg. The joint-displacement sensors are used to detect the real positions of the joints to realize close loop control at joint level, and kinematics computation (the kinematics model of the robot employed in this paper can be found in the authors' previous work [44]). With the multiple sensors fitted, it is convenient to do biomimetic locomotion analyses and realize different kinds of robot motion control schemes.

For such a large-size legged robot walking on unpredictable terrains, the motion stability is of crucial importance and needs to be primarily considered when
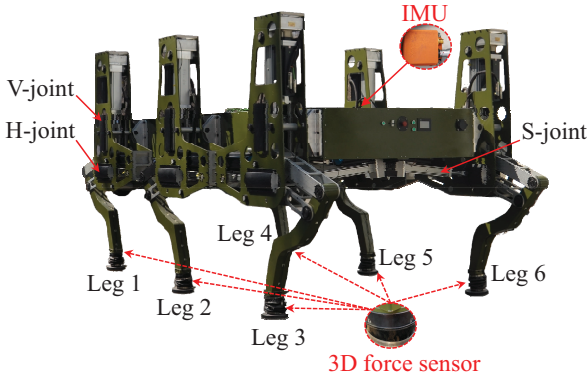
Fig. 1 The whole structure of the large-size hexapod robot with eighteen electrically actuated joints.

Fig. 2 The deterioration of motion caused by the structure deformations and the large contact impacts.

designing the motion control system. Compared with the existing small-size legged robots, the great mass and inertia of the large-size hexapod robot, and the unpredictable terrain conditions, together will cause two main extraordinary problems that are rarely seen on the small-size robots. The two problems which will significantly influence the motion performances of the robot are briefly introduced below.

1. The deformations of the robot: the mass of a small-size legged robot is usually small and therefore it is usually treated as a pure rigid structure, namely the deformations of the robot are usually neglected. But for our large-size hexapod robot with a great mass, the rigid component assumption is no longer applicable and the deformations of the robot will greatly influence the motion altitude and attitude, especially when a commonly used triangle gait form with only three legs supporting the robot body is employed.

2. The great contact impacts between the robot's feet and the unpredictable terrains: the terrains which legged robots move on are usually uneven and unpredictable. Due to the unpredictable terrain conditions, and the robot's large mass property, great contact impacts between the robot's feet and the terrains will occur. The contact impacts will significantly break up the system force equilibrium which plays an important roll in ensuring the balance walking of the robot, and robot body posture deviations will be seen.

Without proper compensation and control applied, these two problems together downgrade the walking performance, as shown in Figure 2, where the blue solid line is the desired body posture, the red dash line represents the actual body posture while the green double dot dash line shows the deformation of robot leg.
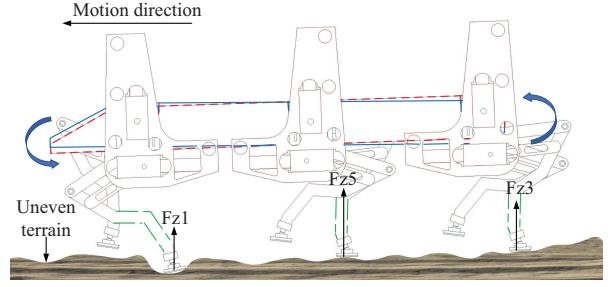
2.2 The problem formulation and the control scheme

As discussed in Section 2.1, to solve these two problems of the large-size hexapod robot, the deformations of the robot cannot be neglected, namely the robot cannot be treated as an ideal rigid structure. Furthermore, the foot forces must be controlled in a compliant way to reduce the contact impacts and ensure the system force equilibrium. To achieve this goal, not only the motion of the legs but also the foot forces must be taken into account at the same time in the design of the control system. Therefore, a proper model which can bridge the gap between the motion of the legs and the foot forces is very essential to be established.

To establish a proper model which can be used for the control process of the large-size hexapod robot, the abstracted spring-muscle model of the EPH may be a good example. In the spring-muscle model, the muscle force can be controlled and the desired dynamics characteristics can be obtained by only appropriately modifying the EPs which are usually represented by the equilibrium positions of the end effector, or the stiffness coefficient. Inspired by the spring-muscle model, in this paper, a simple compliant-leg model which can reflect the deformations of the robot is established. Imitating the spring-muscle model of the EPH, the EP trajectory is defined as a sequence of the robot foot positions.

The deformations of the robot mainly consists of two parts: the deformation of the robot body, and the deformations of the legs. To get a simple model which can be used, all the deformations are treated to be the deformations of the legs. To imitate the situation of deformation, the robot leg is abstracted into a mass-spring-damper model, as shown in Figure 3. It is well to be reminded that only the vertical deformation of the leg is taken into account because the tangential deformation of the leg is really small and has little influence on the moving performance of the robot.

Based on the mass-spring-damper model, the relationship between the foot force and the deformation of the leg can be achieved, as shown in equation (1).
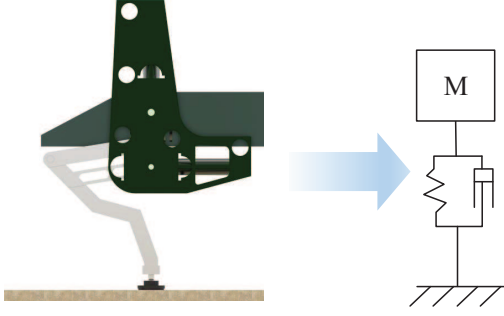
Fig. 3 The abstracted compliant-leg model of the large-size hexapod robot.

$$^{C}F_{iz} = flag_i \cdot {}^{C}f_i = flag_i \cdot (K_{iz} \cdot \Delta^{C}P_{iz} + C_{iz} \cdot \Delta^{C}\dot{P}_{iz}) \tag{1}$$

where $flag_i$ represents the status flag of leg i, if leg i is in stance phase then $flag_i = 1$, otherwise $flag_i = 0$. $^{C}F_{iz}$ represents the vertical foot force of leg i. $^{C}f_i$ represents the equivalent foot force of leg i based on the mass-spring-damper model. $\Delta^{C}P_{iz}$ represents the vertical foot position error of leg i caused by the leg deformation. K_{iz} and C_{iz} represent the equivalent stiffness and damping coefficients, respectively.

Because of the average low moving speed, the motion process of the large-size hexapod robot can be assumed to be quasi-static. Thus, the damping component can be neglected, and equation (1) can be further reduced to equation (2).

$$^{C}F_{iz} = flag_i \cdot {}^{C}f_i = flag_i \cdot K_{iz} \cdot \Delta^{C}P_{iz} \tag{2}$$

The stiffness coefficient K_{iz} is usually easy to get through the method of calibration (the calibration method is introduced in Appendix A). So the key point to solve the problems discussed in section 2.1 is how to control the foot forces in a compliant way to compensate the deformations of the robot and keep the system force equilibrium based on the compliant-leg model. To solve this question, an EP trajectory modification method via a contact-force optimization is developed in this paper, which will be introduced in detail in section 3.

In this method, by establishing the relationship between the desired motion state and the contact foot forces, $\Delta^{C}P_{iz}$ under the desired motion state can be obtained. Furthermore, based on the compliant-leg model, desired contact forces can be calculated. Then with the implementation of an impedance model with force tracking, the final EP trajectory modification value to ensure system force equilibrium, and counter the robot's deformations, can be obtained through a compliant way.

The brief structure of the whole control scheme based on the EP trajectory modification method is shown in Figure 4. Meanings of the parameters in Figure 4 are explained in Table 1.
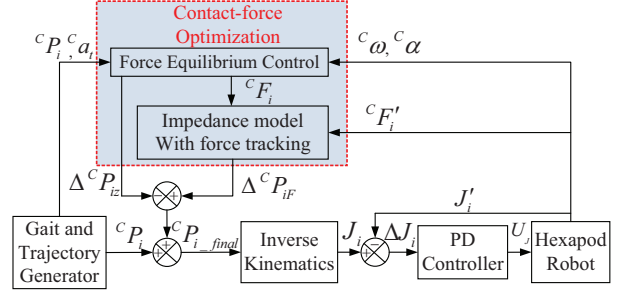

Fig. 4 The brief structure of the control scheme based on the EP modification method in Cartesian space.

Table 1 Important parameters of the EP control scheme.

Parameter	Quantity
$^{C}P_i$	The original foot position vector of leg i
$^{C}a_t$	The desired motion acceleration of the robot
$^{C}\omega$	The actual angular velocity of the robot
$^{C}\alpha$	The actual angular acceleration of the robot
$^{C}F_i$	The desired foot force vector of leg i
$^{C}F_i'$	The actual foot force vector of leg i
$\Delta^{C}P_{iF}$	The force equilibrium EP trajectory modification value
$\Delta^{C}P_{iz}$	The vertical deformation of leg i under system forces
J_i	The desired joint position vector of leg i
J_i'	The actual joint position vector of leg i
ΔJ_i	The joint position deviation
U_J	The control quantity of the joint motor
$^{C}P_{i\_final}$	The final desired EP trajectory

3 The EP trajectory modification via contact-force optimization

For a hexapod robot, the support foot, or namely the foot in stance phase, is the only medium in contact with the external environment and drive the robot to move. Thus, interactive contact forces are of crucial importance for the achievement of the system equilibrium. Nevertheless, the contact forces are always affected by the unknown terrains. The unpredicted interactive dynamic relationship between a robots feet and environment, and the complexity of the terramechanics, together make it hard to control the contact forces directly. A bad contact-force distribution may lead a series of consequences, such as foot sliding, unbalanced momentum on the torso, or even the lost of stability. Aiming

to solve this problem and get an equilibrium system locomotion, a contact-force optimization method is set up to modify the stance-phase EP trajectories in real time. Through the modification method, desired contact forces can be indirectly achieved.

To get an equilibrium motion, the mechanical state of the robot during moving should be analyzed. Figure 5 shows a general motion state of the hexapod robot, in which C represents the robot body coordinate. $^{C}V = \left[^{C}V_x, {}^{C}V_y, {}^{C}V_z\right]^T$ and $^{C}a_t = \left[^{C}a_{tx}, {}^{C}a_{ty}, {}^{C}a_{tz}\right]^T$ represent the motion velocity and acceleration of C. $^{C}\omega = \left[^{C}\omega_x, {}^{C}\omega_y, {}^{C}\omega_z\right]^T$ and $^{C}\alpha = \left[^{C}\alpha_x, {}^{C}\alpha_y, {}^{C}\alpha_z\right]^T$ represent the angular velocity and angular acceleration of C, respectively. $^{C}G = \left[^{C}G_x, {}^{C}G_y, {}^{C}G_z\right]^T$ represents the position of center of mass (COM) in the robot body coordinate frame, namely C coordinate frame. Thus, the acceleration of COM can be written as

$$^{C}a = {}^{C}a_t + {}^{C}\omega \times ({}^{C}\omega \times {}^{C}G) + {}^{C}\alpha \times {}^{C}G \qquad (3)$$

where ^{C}a represents the acceleration of COM. Then the total forces and moments acting on COM can be written as

$$W = \begin{cases} ^{C}F_W = -m{}^{C}a - m\left[0\ 0\ g\right]^T \\ ^{C}M_W = -I{}^{C}\alpha - {}^{C}\omega \times I{}^{C}\omega \end{cases} \qquad (4)$$

where I represents the inertia tensor at COM. W represents the set of the desired virtual force vectors $^{C}F_W$ and moment vectors $^{C}M_W$ acting on COM.

Treating the foot contacting the terrain as a point and neglecting the interactive moments acting on the foot, the motion equilibrium equation of the hexapod robot can be obtained as shown in equation (5),

$$AF + W = 0 \qquad (5)$$

with

$$A = \begin{bmatrix} E & \cdots & E \\ C_1 & \cdots & C_6 \end{bmatrix} \qquad (6)$$

$$F = \left[^{C}F_1{}^T \ \cdots \ {}^{C}F_6{}^T\right]^T \qquad (7)$$

$$^{C}F_i = \left[^{C}F_{ix}, {}^{C}F_{iy}, {}^{C}F_{iz}\right]^T \qquad (8)$$

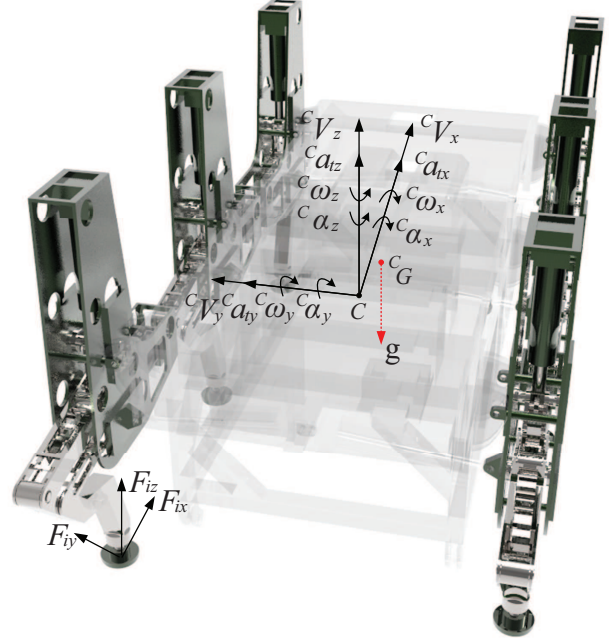$$W = \left[^{C}F_W{}^T \ {}^{C}M_W{}^T\right]^T \qquad (9)$$

Fig. 5 A general motion state and the motion parameters of the hexapod robot.

$$C_i = \begin{bmatrix} 0 & ^{C}G_z - {}^{C}P_{iz} & ^{C}P_{iy} - {}^{C}G_y \\ ^{C}P_{iz} - {}^{C}G_z & 0 & ^{C}G_x - {}^{C}P_{ix} \\ ^{C}G_y - {}^{C}P_{iy} & ^{C}P_{ix} - {}^{C}G_x & 0 \end{bmatrix} \qquad (10)$$

where E represents the 3×3 identity matrix. F represents the set of the desired contact force vectors which is mapped from the foot tip to the COM. $^{C}F_i$ represents the desired contact force vector of leg i, which is mapped from the foot tip to the COM in the three-dimensional Cartesian space.

Equation (5) significantly bridges the gap between the system's desired motion state and the robot contact forces, where the desired forces to ensure system force equilibrium must meet the demand of equation (5). Nevertheless, the order of matrix A is 6×18, and for a hexapod robot, the number of feet in the stance phase must not be less than three. Therefore, the achievement of a unique solution of the desired foot forces which can meet the demand of equation (5) has become a redundancy problem. To solve this problem, additional constraints are needed.

For controllers based on inverse dynamics, solving this problem is usually transformed into solving a quadratic programming (QP) problem. A nonlinear optimization goal based on the inverse dynamics model of the robot, like minimization of the energy consumption, is usually established. Then equality constraint like equation (5), and inequality constraints are additional defined to make the redundancy problem match the stan-

dard form of a QP problem. By solving the QP problem, a unique solution of the desired contact forces which can meet the demand of system force equilibrium can be obtained.

Although the inverse dynamics controllers can solve this redundancy problem, as discussed in the introduction section, the inverse dynamics modeling is usually complex and full of nonlinear computations. When the robot's configuration is complex, this problem becomes worse. In the authors' previous work [44], a linear foot force distribution algorithm is attempted to solve the redundancy problem. But in that algorithm, an obvious defect can be found through mathematical analysis. The foot force distribution algorithm cannot ensure system force equilibrium for all the support forms of the hexapod robot. For example, when support form C showed in Figure 4 in reference [44] is employed as the current gait form, none of the constraints for the three situations showed in Figure 7 in reference [44] can be used. Similar problems can be found in other support forms. The system force equilibrium cannot be ensured mathematically for all the support forms.

To reduce the complexity of computation, and get a unique solution of the desired contact forces which can ensure system force equilibrium for all the support forms of the hexapod robot, in this paper, constraints based on deformation compatibility equation, foot-sliding resistance and internal-force elimination are proposed to solve the redundancy problem.

The deformation compatibility equation is set up based on the compliant-leg model, namely equation (2). Assuming that under the function of forces and moments acting on the body, the robot body makes tiny movements, and there is no position change of the robot foot with respect to the ground, then the position change of the robot foot with respect to the robot body can be written in the form shown in equation (11).

$$\Delta^C P_i = R_W{}^C P_i - {}^C P_i + \Delta Q \tag{11}$$

with

$$R_W \approx \begin{bmatrix} 1 & \Delta\beta\Delta\gamma - \Delta\alpha & \Delta\beta + \Delta\alpha\Delta\gamma \\ \Delta\alpha & \Delta\alpha\Delta\beta\Delta\gamma + 1 & \Delta\alpha\Delta\beta - \Delta\gamma \\ -\Delta\beta & \Delta\gamma & 1 \end{bmatrix} \tag{12}$$

where $\Delta^C P_i = \left[\Delta^C P_{ix}, \Delta^C P_{iy}, \Delta^C P_{iz}\right]^T$ represents the position change of the robot foot i. $\Delta\alpha$, $\Delta\beta$ and $\Delta\gamma$ represent tiny yaw, pitch and roll angular changes of the robot body, respectively. $\Delta Q = [\Delta Q_x, \Delta Q_y, \Delta Q_z]^T$ represents the three tiny displacements of the robot body.

Thus, based on equation (2), equation (11) and equation (12), $\Delta^C P_{iz}$ and the deformation compatibility equation can be achieved, as shown in equation (13) and equation (14), respectively.

$$\Delta^C P_{iz} = -\Delta\beta\,^C P_{ix} + \Delta\gamma\,^C P_{iy} + \Delta Q_z \tag{13}$$

$$
\begin{aligned}
{}^C F_{iz} = &-(flag_i K_{iz}{}^C P_{ix})\Delta\beta + (flag_i K_{iz}{}^C P_{iy})\Delta\gamma \\
&+(flag_i K_{iz})\Delta Q_z
\end{aligned}
\tag{14}
$$

Walking straight forward is the most important moving state of the hexapod robot. It is mainly driven by the tangential contact forces along the robot moving direction, namely $^C F_{ix}$. To keep a stable walking of the robot, foot-sliding resistance is taken into account for the calculation of $^C F_{ix}$. To reduce the risk of foot sliding, the maximum ratio of the tangential force to the normal force should be as small as possible. According to [45], this goal can be reached by making the ratio of every support leg equals to the ratio of the total tangential forces to the total normal forces. Therefore, $^C F_{ix}$ can be calculated using equation (15).

$$^C F_{ix} = \mu\,^C F_{iz} \tag{15}$$

with

$$\mu = {}^C F_{Wx}/{}^C F_{Wz} \tag{16}$$

where $^C F_{Wx}$ represents the sum of all $^C F_{ix}$. $^C F_{Wz}$ represents the sum of all $^C F_{iz}$.

To calculate the other component of the tangential force, namely $^C F_{iy}$, internal-force elimination is taken into account to improve the durability of the robots mechanical components. Just like the normal contact force, to distinguish whether the foot is in stance phase or not, $^C F_{iy}$ is defined as

$$^C F_{iy} = flag_i \cdot {}^C f_{iy} \tag{17}$$

where $^C f_{iy}$ represents the alternative contact force of leg i along the y direction.

The two legs assembled in the middle of the robot body, namely leg 2 and leg 5, have little effect on the yaw angle change of the body, the yaw angle change is mainly driven by the other four legs. So in order to reduce the internal force between legs, a constraint is set up, as shown in equation (18).

$$\begin{cases} {}^C f_{1y} = {}^C f_{4y} \\ {}^C f_{3y} = {}^C f_{6y} \end{cases} \qquad (18)$$

The constraint for the middle two contact forces is set up as shown in equation (19).

$$\begin{cases} {}^C F_{2y} = \dfrac{flag_2}{flag_1 + flag_2 + flag_3} {}^C F_{Wy} \\ {}^C F_{5y} = \dfrac{flag_5}{flag_4 + flag_5 + flag_6} {}^C F_{Wy} \end{cases} \qquad (19)$$

Thus, based on equation (5) to equation (19), a system of linear equations can be achieved, as shown in equation (20).

$$
\begin{aligned}
B \cdot x & \\
= & \begin{bmatrix} flag_1 & flag_3 & flag_4 & flag_6 & 0 & 0 & 0 \\ 0 & 0 & 0 & 0 & b_{25} & b_{26} & b_{27} \\ b_{31} & b_{32} & b_{33} & b_{34} & b_{35} & b_{36} & b_{37} \\ 0 & 0 & 0 & 0 & b_{45} & b_{46} & b_{47} \\ b_{51} & b_{52} & b_{53} & b_{54} & b_{55} & b_{56} & b_{57} \\ 1 & 0 & -1 & 0 & 0 & 0 & 0 \\ 0 & 1 & 0 & -1 & 0 & 0 & 0 \end{bmatrix} \begin{bmatrix} {}^C f_{1y} \\ {}^C f_{3y} \\ {}^C f_{4y} \\ {}^C f_{6y} \\ \Delta\beta \\ \Delta\gamma \\ \Delta Q_z \end{bmatrix} \\
= & \begin{bmatrix} -{}^C F_{Wy} - {}^C F_{2y} - {}^C F_{5y} \\ -{}^C F_{Wz} \\ -{}^C M_{Wx} + ({}^C P_{2z} - {}^C G_z){}^C F_{2y} + ({}^C P_{5z} - {}^C G_z){}^C F_{5y} \\ -{}^C M_{Wy} \\ -{}^C M_{Wx} - ({}^C P_{2x} - {}^C G_x){}^C F_{2y} - ({}^C P_{5x} - {}^C G_x){}^C F_{5y} \\ 0 \\ 0 \end{bmatrix} \\
= & \; b
\end{aligned}
$$
$$(20)$$

where the unknown coefficients of matrix B are explained in Table 2.

It can be verified that for all gait types of a hexapod robot listed in reference [44], equation (21) can be satisfied. Namely, a unique solution of equation (20) can be achieved. When the solution x of equation (20) is obtained, desired contact forces of all legs in stance phase can be finally calculated according to equation (14), equation (15), equation (17) and equation (19). The system force equilibrium can be ensured for all gait types during walking.

$$rank[B] = rank[B, b] = 7 \qquad (21)$$

Although the desired contact forces for the system equilibrium can be obtained through the method proposed above, it is still hard to get a good contact force tracking performance through a direct way. Direct force close-loop control method may cause the system unstable due to the sensitivity and noises of the foot force sensors equipped. To solve this problem, a position-based impedance control model with force tracking is used, as shown in equation (22).

$$\Delta F_i = M_d \Delta^C \ddot{P}_{iF} + C_d \Delta^C \dot{P}_{iF} + K_d \Delta^C P_{iF} \qquad (22)$$

where ΔF_i represents foot force deviation of leg i between the actual foot force ${}^C F_i'$ and the desired foot force ${}^C F_i$. $\Delta^C P_{iF}$ represents the EP trajectory modification value, namely foot position modification value. M_d, C_d and K_d represent the user-defined impedance coefficients, respectively.

The EP trajectory modification method via contact-force optimization proposed here is more like biological behaviors of the legged creatures or humans. Legged creatures or humans can optimize contact forces according to the motion state wanted. This optimization is finally achieved by changing foot motion trajectories. For example, if a human steps on a soft terrain and a large contact force is needed to keep the body balance, deeper foot position will be taken. Through this control method, not only the system equilibrium but also a compliance interaction between the robot foot and terrain can be obtained.

To make the whole control logic clearly in detail, Figure 4 is extended into Figure 6, where the color circled numbers, namely the green circled 1 and the red circled 2, represent the signal tunnels that pass the same signal. Eq.(n) in Figure 6 represents equation (n).

4 Experiments and result discussions

To verify the effectiveness of the control scheme in improving the walking performance and ensuring the walking stability, several experiments were carried out on the real large-size hexapod robot. First, a common rigid flat terrain walking experiment was carried out to demonstrate the effectiveness of the control scheme in compensating the robot's deformations. Second, an artificial soft terrain walking experiment was carried out to demonstrate the advantages of the control scheme in terrain deformation counteraction and keeping the stable walking attitude. Third, a natural field walking experiment was carried out to verify the practical engineering application performance of the control scheme.

The hexapod robot is equipped with an industrial PC controller from Beckhoff with an i5 CPU and a real-time control system inside. Fast data exchanges can be ensured by using the Ethernet. The motion control program is written in the combination of the C++ language and PLC language on TwinCAT 3 platform.

Table 2 The unknown coefficients of matrix B.

Parameter	Value	Parameter	Value
b_{25}	$-\sum_{i=1}^{6} flag_i K_{iz}{}^C P_{ix}$	b_{26}	$\sum_{i=1}^{6} flag_i K_{iz}{}^C P_{iy}$
b_{27}	$\sum_{i=1}^{6} flag_i K_{iz}$	b_{31}	$-flag_1({}^C P_{1z} - {}^C G_z)$
b_{32}	$-flag_3({}^C P_{3z} - {}^C G_z)$	b_{33}	$-flag_4({}^C P_{4z} - {}^C G_z)$
b_{34}	$-flag_6({}^C P_{6z} - {}^C G_z)$	b_{35}	$-\sum_{i=1}^{6} flag_i K_{iz}{}^C P_{ix}({}^C P_{iy} - {}^C G_y)$
b_{36}	$\sum_{i=1}^{6} flag_i K_{iz}{}^C P_{iy}({}^C P_{iy} - {}^C G_y)$	b_{37}	$\sum_{i=1}^{6} flag_i K_{iz}({}^C P_{iy} - {}^C G_y)$
b_{45}	$-\sum_{i=1}^{6} flag_i K_{iz}{}^C P_{ix}[\mu({}^C P_{iz} - {}^C G_z) - ({}^C P_{ix} - {}^C G_x)]$	b_{46}	$\sum_{i=1}^{6} flag_i K_{iz}{}^C P_{iy}[\mu({}^C P_{iz} - {}^C G_z) - ({}^C P_{ix} - {}^C G_x)]$
b_{47}	$\sum_{i=1}^{6} flag_i K_{iz}[\mu({}^C P_{iz} - {}^C G_z) - ({}^C P_{ix} - {}^C G_x)]$	b_{51}	$flag_1({}^C P_{1x} - {}^C G_x)$
b_{52}	$flag_3({}^C P_{3x} - {}^C G_x)$	b_{53}	$flag_4({}^C P_{4x} - {}^C G_x)$
b_{54}	$flag_6({}^C P_{6x} - {}^C G_x)$	b_{55}	$\sum_{i=1}^{6} flag_i K_{(iz)}{}^C P_{ix}\mu({}^C P_{iy} - {}^C G_y)$
b_{56}	$-\sum_{i=1}^{6} flag_i K_{iz}{}^C P_{iy}\mu({}^C P_{iy} - {}^C G_y)$	b_{57}	$-\sum_{i=1}^{6} flag_i K_{iz}\mu({}^C P_{iy} - {}^C G_y)$
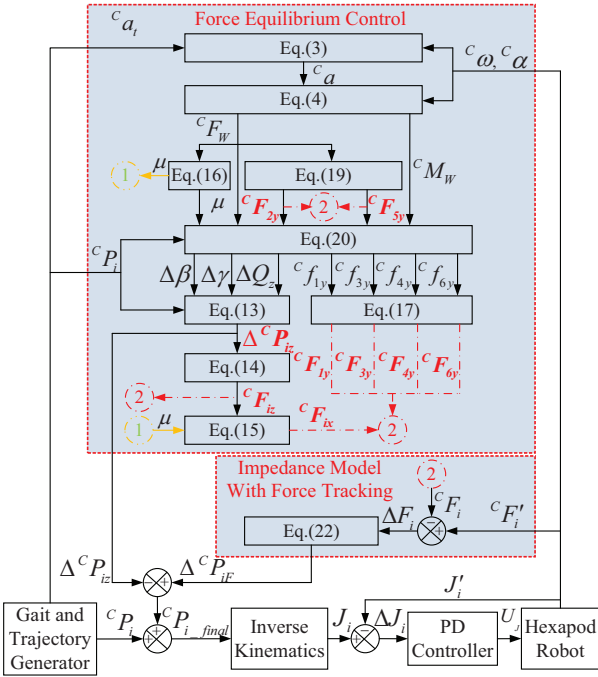
Fig. 6 The detailed EP control scheme.

It is well to be noticed that only triangle gait form was employed in the three experiments (about the stable hexapod gait forms, see the authors' previous work [46]). The triangle gait form is most commonly used for hexapod robots. A hexapod robot walking with a triangle gait form can be more sensitive to the deformations of the robot and the terrain changes because only three legs are supporting the robot body at the same time during walking. Besides, although the walk-

ing stability may be increased with the increase in the number of support legs, this will also cause the problem of walking decay [47]. Therefore, the triangle gait form is more proper to be employed to exam the walking performance.

To demonstrate the walking improvement of the robot using the EP control scheme better, during every experiment, walking only with the kinematics control scheme (WKC), and walking with a typical inverse dynamics control scheme (WID) were employed as comparisons with walking with the EP control scheme (WEP). In the former two experiments, no special contact detection was employed in the three control schemes. In the third experiment, to ensure a safe walking, a simple contact detection was employed which will be briefly introduced in section 4.3. The control schemes of WKC and WID are shown in Figure 7.

It is well to be noticed that for the WID control scheme in Figure 7(b), only the force equilibrium control part of WEP in Figure 4 is replaced by a force distribution QP solver based on inverse dynamics. Through this way, the influence on the walking performance caused by the parameter changes will be reduced. The force distribution QP solver was employed from reference [48]. This is a typical inverse dynamics solver. Similar solvers can be found in other works, such as reference [15] and reference [16]. J_{i_ori}, $\dot{J}_{i\_ori}$, and $\ddot{J}_{i\_ori}$ in Figure 7(b) represent the original joint position, joint velocity, and joint acceleration vector of leg i, respectively. The inverse dynamics modeling process of the large-size hexapod robot can be seen in the authors' previous work [49].

Table 3 Global parameters for the experiments.

Parameter	Quantity	Value
$K_{iz} = [K_{1z}, K_{2z}, K_{3z}, K_{4z}, K_{5z}, K_{6z}]$	Vertical stiffness coefficient of the leg	$[146, 325, 177, 149, 327, 175]$ kN $\cdot$ m^{-1}
K_d	Stiffness coefficient of the impedance model	120 kN $\cdot$ m^{-1}
C_d	Damping coefficient of the impedance model	20 kN $\cdot$ m^{-1} $\cdot$ s
M_d	Inertia coefficient of the impedance model	3000 kg

(a)

(b)
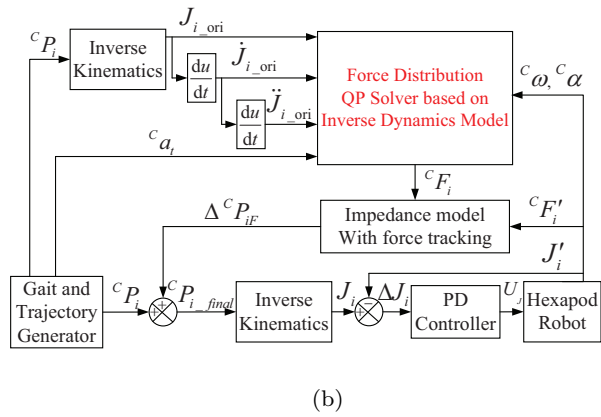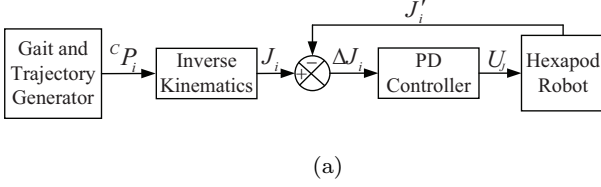
Fig. 7 The brief structures of the kinematics control scheme and the inverse dynamics control scheme: (a) the kinematics control scheme, and (b) the inverse dynamics control scheme.

Some global parameters used in the experiments are shown in Table 3.

4.1 The rigid flat terrain walking experiment

The walking parameters used in this experiment is shown in Table 4. In Table 4, the duty factor represents the ratio of the support time to the cycle time. The cycle time represents the time period for a leg to complete a swing and a support phase. The motion velocity of the robot can be calculated using equation (23).

$$V_x = \frac{S_x}{\lambda \cdot T} \tag{23}$$

The walking process is shown in Figure 8. The terrain is the most commonly seen rigid cement concrete pavement. During walking, the deformation of the terrain can be neglected. The triangular support regions bounded by the yellow lines show the changes of the

Table 4 Walking parameters.

Parameter	Quantity	Value
S_x	Step length	400 mm
T	Cycle time	8 s
λ	Duty factor	0.5
h	Step height	120 mm

support legs during walking. The comparative experiment result of the robot body attitude changes is shown in Figure 9.

During the experiment, the desired pitch and roll angles were set the same to 0 degree while the desired body height was set to 1380 mm. Based on the previous experience in laboratory commissioning tests of the robot, a stable motion range for the robot's pitch and roll angles is set to ± 1.5 degrees to evaluate the motion performances, just as the range between the two black double dot-dash lines shown in Figure 9(b).

It can be analyzed from Figure 9 that although the robot can move within the stable motion range, the pitch angle, roll angle, and body height of WKC fluctuate significantly. The fluctuations seem at a low-value level, but for a large-size robot, macroscopic posture changes during the robot walking can be seen. Because the deformation of the rigid terrain can be nearly neglected, therefore without any regulation of the EP trajectories, the body attitude fluctuations are mainly caused by the deformations of the robot body and legs. This phenomenon matches the deformation assumption of the large-size robot and can provide a realistic basis for the abstracted compliant-leg model, namely equation (2).

Compared with WKC, the walking performances were significantly improved by WID and WEP. The max absolute tracking error of the pitch angle was reduced from 0.86 degree (WKC) to 0.41 degree (WID), and 0.37 degree (WEP), respectively. The max absolute tracking error of the roll angle was reduced from 1.08 degrees (WKC) to 0.58 degree (WID), and 0.49 degree (WEP), respectively. The standard deviation of the pitch angle was reduced from 0.28 degree (WKC) to 0.12 degree (WID), and 0.08 degree (WEP), respectively. The standard deviation of the roll angle was reduced from 0.37 degree (WKC) to 0.18 degree (WID),
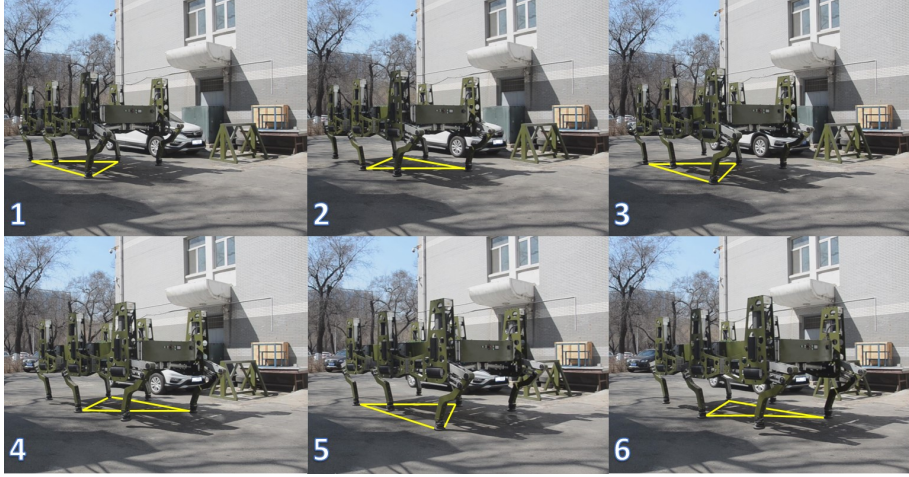
Fig. 8 The snapshots of the rigid flat terrain walking process.
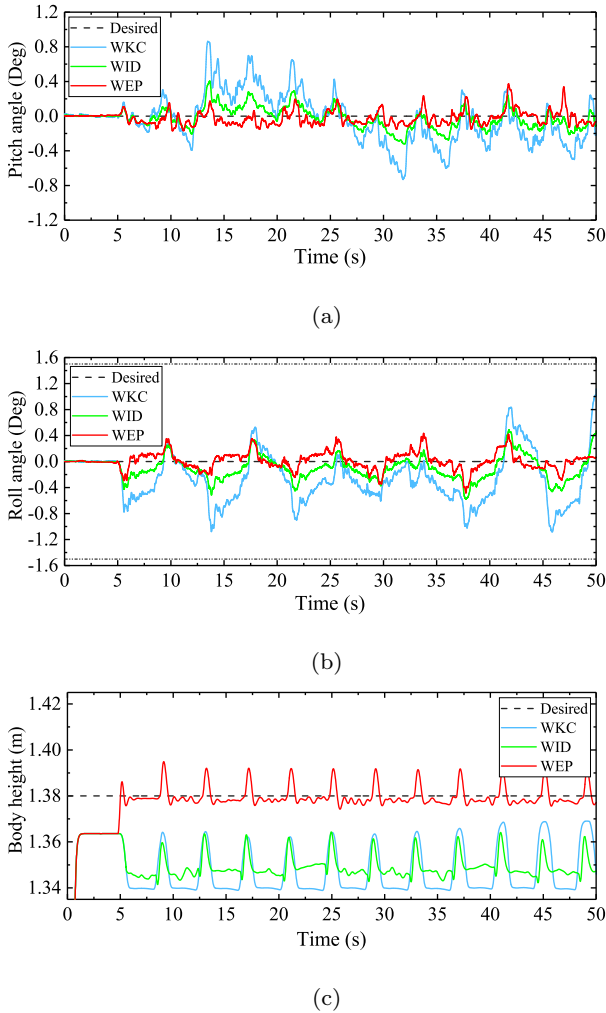

(a)

(b)

(c)

Fig. 9 The robots body attitude comparisons as a result of the rigid flat terrain walking experiment: (a) the body pitch angle comparison, (b) the body roll angle comparison and (c) the body height comparison.

and 0.13 degree(WEP), respectively. The max absolute tracking error of the body height was reduced from 41.13 mm (WKC) to 38.53 mm (WID), and 14.92 mm (WEP), respectively. The standard deviation of the body height was reduced from 9.85 mm (WKC) to 4.81 mm (WID), and 4.01 mm (WEP), respectively. (The body height measuring method is introduced in Appendix B).

The disparate control performance mainly results from the different system states brought by the different control schemes. In contrast to the common system of WKC, the robot system equilibrium can be more easily obtained using the WID and WEP control schemes. Taking the robot roll angle variations for instance, the roll angle fluctuation state is mainly determined by the foot force relationship of the left and right supporting legs. Therefore, F_{z5}, namely vertical foot force of leg 5, is set in comparison with $F_{z1} + F_{z3}$, namely the sum of the vertical contact forces of leg 1 and leg 3, as shown in Figure 10.

Figure 10 shows the vertical foot force comparisons of WKC, WID, and WEP during the same three stance phases, respectively. During a steady stance phase, if a stable roll angle is desired to be achieved, $F_{z1} + F_{z3} \approx F_{z5}$ should be satisfied. But as shown in Figure 10(a), when the common control scheme, namely WKC is employed, the foot force deviation between $F_{z1} + F_{z3}$ and F_{z5} is very obviously seen. The foot force deviation is mainly caused by the deformations of the robot body and legs. Leg 5 is the only support leg on one side of the robot body. Compared with leg 1 and leg 3, the large payload will easily cause more deformation of leg 5. The force equilibrium of the robot can hardly be achieved if no regulation of the system is introduced.

In contrast to the force relationship of WKC, force equilibrium of the robot system can be nearly satisfied
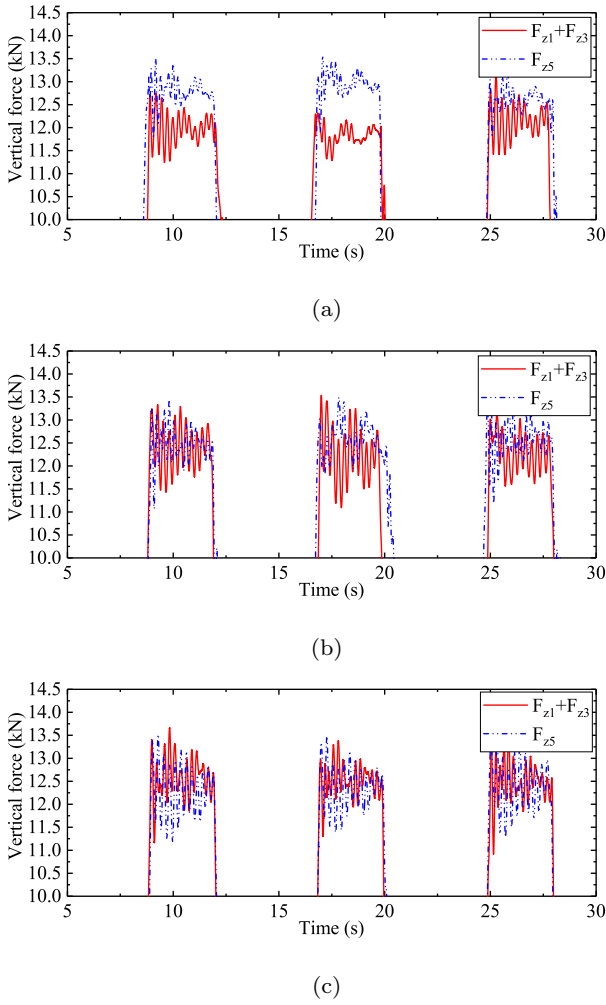
Fig. 10 The vertical foot force comparisons: (a) the vertical foot force comparison of WKC, (b) the vertical foot force comparison of WID, and (c) the vertical foot force comparison of WEP.

under the function of WID and WEP, as shown in Figure 10(b) and Figure 10(c). The force ratio of $F_{z1} + F_{z3}$ to F_{z5} can almost maintain unchanged and the sum of the three legs vertical contact forces is almost steady at 25 kN during the stance phases. In other words, the sum of the supporting legs' vertical contact forces almost equals to the gravity of the robot. During any common stance phase of each walking cycle, $F_{z1} + F_{z3} \approx F_{z5}$ can be satisfied, which means the robot is force balanced in the coronal plane. Because of the balanced contact forces during the stance phase, the amplitude fluctuation of the robot's roll angle is small. System equilibrium can be ensured.

Although both the WID and WEP system can ensure system force equilibrium during the flat terrain walking, there is still a significant gap between them in regulating body height. As an instance, Figure 11

shows the vertical foot position comparison of leg 5 during two support phases under the three control schemes to demonstrate the advantage of the WEP system in robot body height regulation. (The actual vertical foot position computation is introduced in Appendix B, equation (27).) Because no contact detection algorithm is employed in the three control schemes, obvious foot position changes caused by the foot force fluctuations can be seen in Figure 11 when leg status switches. These foot position changes will cause the robot body height changes, which can be seen from Figure 9(c). During the flat terrain walking, the desired body height is 1380 mm. Ideally, if the desired robot body height is wanted to be ensured, the vertical foot position of all the support legs with respect to the body coordinate C should be -1380 mm. But it can be seen from Figure 11 that both the WKC and WID system cannot meet this demand. Take a steady period of the first support phase for instance to analyze the foot position improvement quantitativly, namely the grey area from $t_1 = 9.2$ s to $t_2 = 12.2$ s in Figure 11. The average vertical foot positions of leg 5 under WKC, WID, and WEP systems during this period are -1339.10 mm, -1346.91 mm, and -1380.42 mm, respectively. Compared with WKC and WID, due to the deformation compensation, the vertical foot position of WEP can almost track the ideal value with little deviation. This is why the robot body height of WEP can be regulated much better than the other two control schemes.
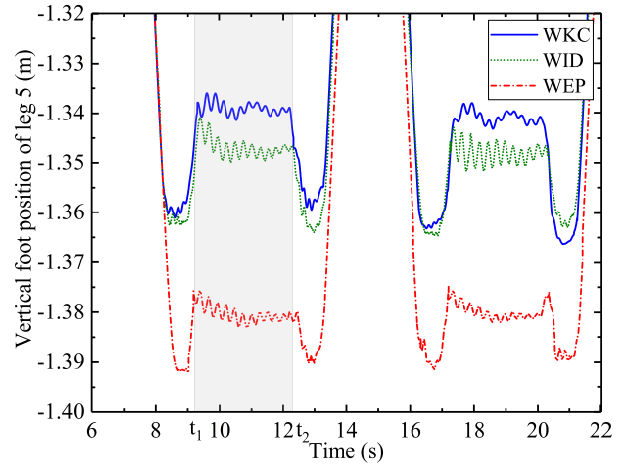

Fig. 11 The vertical foot position comparison of leg 5 under the three control schemes.

This different control performance is mainly caused by the deformations of the robot. Although the foot position of leg 5 of WID can be regulated through the regulation of foot forces, it can still not compensate the robot deformations to ensure the desired body height.

As a comparison, under the function of the EP control scheme, the leg deformation, namely $\Delta^C P_{iz}$, can be computed in advance, and compensated through a feed-forward way. Therefore, the robot body height can be ensured. It can be inferred that with the growth of the robot's mass and payload, the deformations of the robot will increase. When facing this situation, the advantage of the EP control scheme proposed will be more significant.

4.2 The artificial soft terrain walking experiment

The results of the rigid flat terrain walking experiment verified the effectiveness of the EP control scheme in counteracting the large-size hexapod robots deformations. But in fact, the terrains on which the legged robots always walk cannot be as flat or rigid as desired, and they are usually soft with obvious deformations and uneven with topographic fluctuations. Unknown disturbances caused by the deformation and the roughness of the terrain will lead to a more unstable motion performance. To verify the effectiveness of the EP control scheme in improving the robots walking stability on the uneven soft terrain, an artificial soft terrain walking experiment was carried out. The walking parameters are shown in Table 5.

Table 5 Walking parameters.

Parameter	Quantity	Value
S_x	Step length	400 mm
T	Cycle time	10 s
λ	Duty factor	0.5
h	Step height	150 mm

The artificial soft terrain which was constructed of EPE plates and plywood plates is shown in Figure 12. Each piece of the soft EPE plates is 1 m×1 m×20 mm while each of the hard plywood plates is 0.7 m×0.5 m×22 mm (Figure 12 shows some acceptable manufacturing errors in thickness). The basement of this terrain was constructed with two layers of the blue EPE plates shown in Figure 12. Several yellow EPE plates were randomly placed on and besides the basement. The highest part of the terrain was constructed with five layers of the EPE plates. Because the EPE plate is soft and can produce noticeable deformation when being compressed, therefore it is very suitable to be employed to simulate the deformation of the terrain. The plywood plates are placed to simulate the hard parts of the terrain to make the experiment more natural. The same comparative control schemes, namely WKC and WID

showed in Figure 7, were employed to make a comparison with the EP control scheme proposed. The walking process is shown in Figure 13.
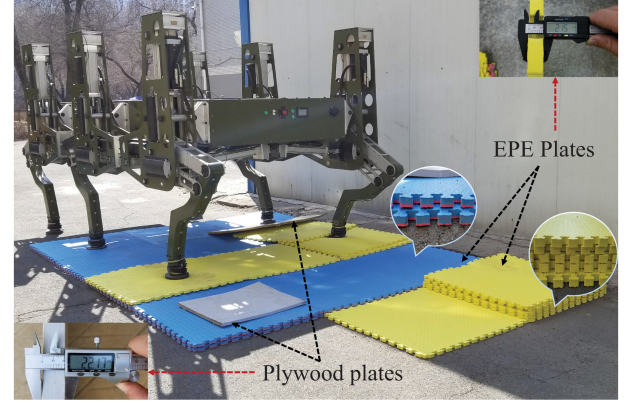

Fig. 12 The artificial soft terrain constructed of EPE plates and plywood plates.

During walking, the soft terrain was easily compressed with obvious deformation, as shown in Figure 14. Compared with the rigid terrain walking, the deformations of the terrain and the robot itself will together lead to a more unstable motion if no compensation is employed into the control system. This bad situation can be seen through the attitude changes of the robot, as shown in Figure 15.

It can be seen from Figure 15 that compared with the rigid flat terrain walking experiment, the robot's pitch and roll angles fluctuate even more sever during walking with WKC. During some periods of walking, the pitch and roll angles move out of the stable range. This phenomenon matches the guess that the deformations of the terrain and the robot itself will seriously influence the walking stability. As a comparison with the walking performance of WKC, the robot achieved more stable walking performances under WID and WEP systems. The fluctuations of the robot's pitch and roll angles reduced significantly. The max absolute tracking error of the pitch angle was reduced from 1.83 degrees (WKC) to 0.75 degree (WID), and 0.65 degree (WEP), respectively. The standard deviation of the pitch angle was reduced from 0.79 degree (WKC) to 0.32 degree (WID), and 0.15 degree (WEP), respectively. The max absolute tracking error of the roll angle was reduced from 2.21 degrees (WKC) to 1.24 degrees (WID), and 1.19 degrees (WEP), respectively. The standard deviation of the roll angle was reduced from 0.86 degree (WKC) to 0.36 degree (WID), and 0.22 degree (WEP), respectively. The pitch and roll angles were controlled within the stable range during the motion processes of WID and WEP.
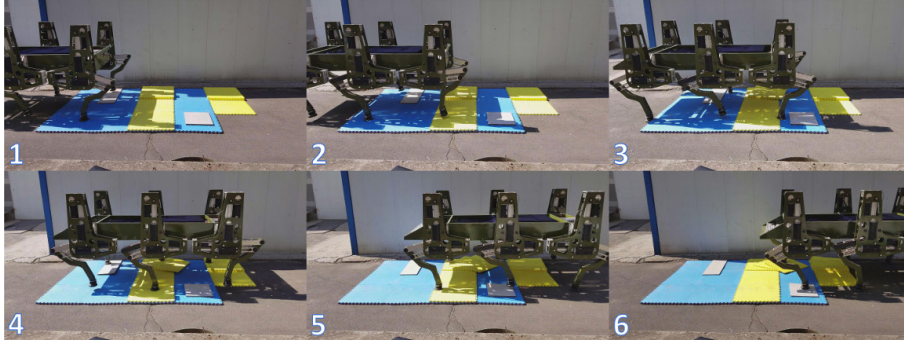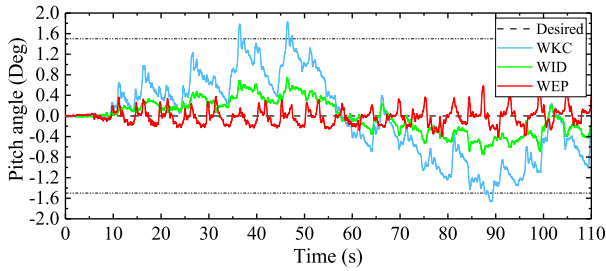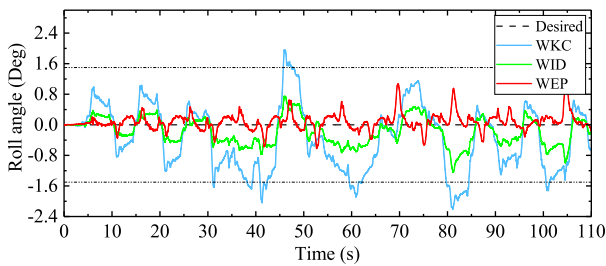
Fig. 13 The snapshots of walking on the artificial soft terrain surfaces.

Fig. 14 The deformation of the artificial soft terrain.

(a)

(b)

Fig. 15 The robot's body attitude comparisons as a result of the artificial soft terrain walking experiment: (a) the body pitch angle comparison and (b) the body roll angle comparison.

Similar to the rigid flat terrain walking experiment, Figure 16 shows the vertical foot force comparisons of WKC, WID, and WEP during the same five stance phases as an instance to explain the roll angle improvement. It can be seen from Figure 16(a) that compared with the rigid flat terrain walking, the foot forces of the support legs fluctuated more sever during walking on the uneven artificial soft terrain with WKC system. The foot force balance was significantly broken. This is why big roll angle fluctuation can be seen in Figure 15(b). When WKC was replaced by WID and WEP, obvious improvements of the vertical foot force relationship can be seen from Figure 16(b) and Figure 16(c). Although compared with the rigid flat terrain walking, $F_{z1} + F_{z3} \approx F_{z5}$ cannot be ideally ensured under both WID and WEP systems due to the deformation and uneven characteristic of the artificial soft terrain, the fluctuations of the vertical foot forces were significantly reduced. Compared with WKC, the deviations between $F_{z1} + F_{z3}$ and F_{z5} were obviously reduced when WID and WEP were employed. Therefore, the motion performances were improved.

It can be seen from the experiment results shown in Figure 15 and Figure 16 that compared with WID, the walking performance of WEP is improved, even though the improvement is not very big. But in the EP control scheme proposed, no nonlinear inverse dynamics model was employed. As discussed in the introduction part, the inverse dynamics modeling process is usually quite complex. Besides, compared with the complex QP solver commonly employed by the traditional inverse dynamics controllers, the computation process of the foot forces ensuring system force equilibrium in the EP control scheme proposed is quite simple. The whole control scheme is totally linear. Therefore, achieveing the same stable control performance, the EP control scheme proposed is more simple to be employed.
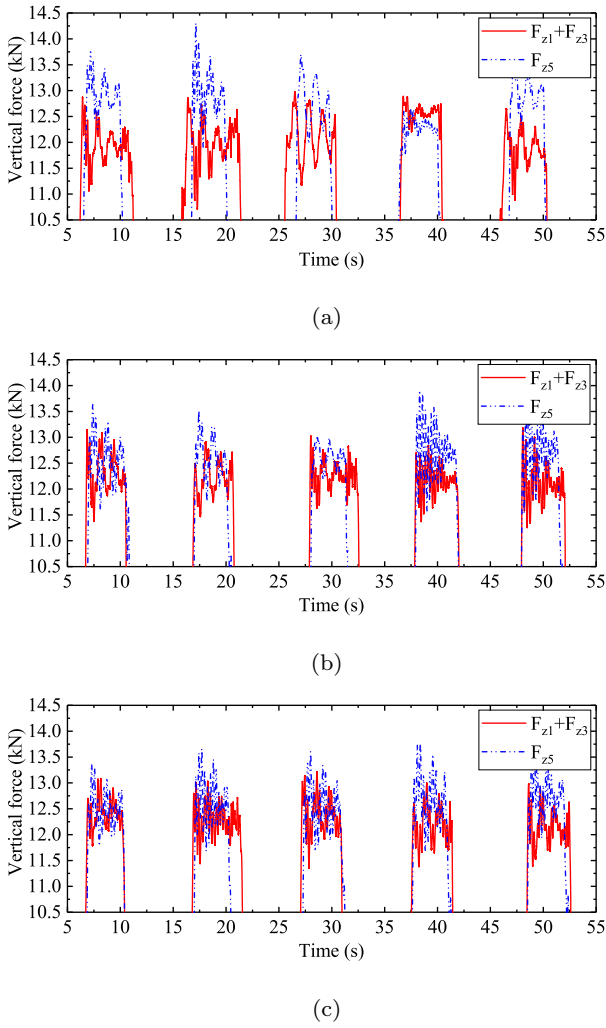
(a)

(b)

(c)

Fig. 16 The vertical foot force comparisons: (a) the vertical foot force comparison of WKC, (b) the vertical foot force comparison of WID, and (c) the vertical foot force comparison of WEP.

4.3 The natural field walking experiment

From the theoretical analysis and the experiment result analyses above, the advantages of the EP control scheme in walking posture regulation and simple computation have been demonstrated. To finally test the applicability of the EP control scheme in ensuring stable motion of the robot in a real natural environment, a natural field walking experiment was carried out. In this experiment, only the EP control scheme was employed. The natural field is shown in Figure 17. The natural field is constructed with several randomly placed holes dug on an irregular slope topography. The soil of the field is soft and can lead to obvious foot sinkages of the robot during walking. The depth of the holes is 200 mm. Due to the depth of the holes, to ensure a safe walking process, a simple contact detection was employed.

A rest time period of 3 seconds is set between each triangle step. During the rest time, the robot will maintain steady with six legs supporting the body. Due to the function of the EP control scheme, the desired foot forces of the legs will be computed. If one swing leg steps into the hole at the leg status switching time, the desired foot force won't be reached. Then under the function of the impedance model in the EP control scheme, a deeper step will be taken until the desired foot force is reached. During the reaching time, the other legs will keep their positions unchanged. Once the desired foot force is reached, the robot will take the next triangle step to move forward. The walking parameters during this experiment are shown in Table 6.

Fig. 17 The real field test irregularities with random holes.

Table 6 Walking parameters.

Parameter	Quantity	Value
S_x	Step length	340 mm
T	Cycle time	10 s
λ	Duty factor	0.5
h	Step height	150 mm

It is well to be noticed that in this experiment, the slope angle of the field is natural and uneven. During walking, the body of the robot was always parallel to the slope. So the desired pitch angle in this experiment was as same as the slope angle. The slope angle was obtained using a macro terrain recognition method in the authors' previous work [46]. The walking process of the robot is shown in Figure 18.

As shown in Figure 18, the body of the robot is leaning during the walking process because of the time-varying slope angle. The actual pitch and roll angles of the robot during the natural field walking is shown in Figure 19. The range between the black double dot-dash lines is the stable motion range. It can be seen that during the walking process, the pitch and roll an-
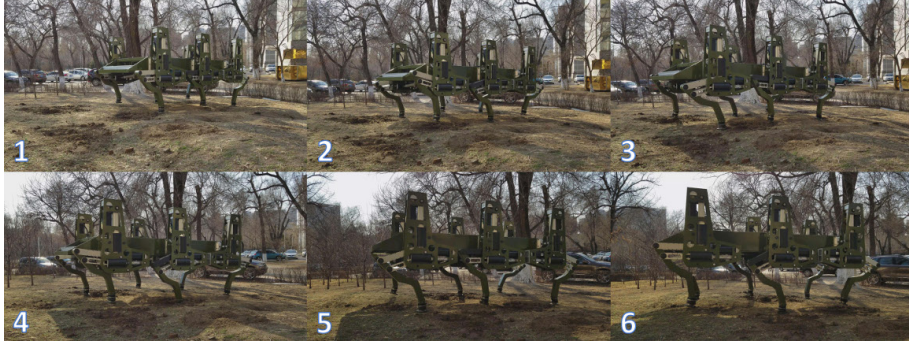
Fig. 18 The snapshots of the natural field walking process.
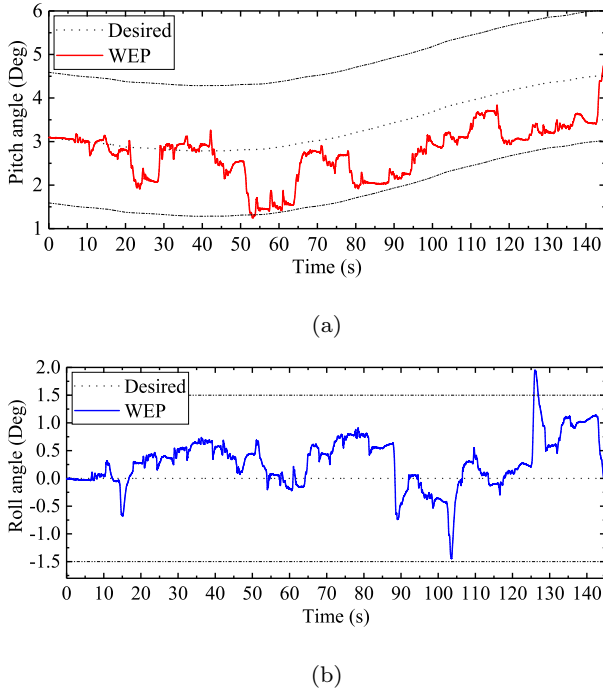

(a)

(b)

Fig. 19 The robot's body attitude changes as a result of the natural field walking experiment: (a) the body pitch angle change and (b) the body roll angle change.

gles are almost within the stable motion ranges. The pitch angle can almost track the desired value, namely, the slope angle detected. The max absolute tracking errors of the pitch and roll angles are 1.57 degrees and 1.95 degrees, respectively. The tracking errors beyond the stable motion range are caused by the sudden foot slippage due to the unstable landing angle of the foot in the hole, and the foot sinkage due to the soft soil in the hole. The foot landing angle of the robot employed in this article cannot be controlled because the ankle joint is a passive joint. Furthermore, in a real natural environment, the detailed terrain roughness information is hard to be obtained unless specific sensors are equipped on the robot. Excluding the uncontrolled fac-

tors, the robot can achieve a stable motion under the function of the EP control scheme proposed.

Figure 20 shows the vertical foot positions of leg 1, leg 3 and leg 5 with respect to the robot body coordinate C. During one stance phase of this experiment, leg 1, leg 3 and leg 5 supported the robot body at the same time and drove the robot to move forward. Because of the EP control scheme proposed, the vertical foot positions of the three legs are not the same and keep changing during the walking process. Obvious foot trajectory modifications, namely the EP trajectory modifications can be seen in Figure 20. The EP trajectory modifications enable the robot to adapt to the terrain changes, and therefore the walking stability can be ensured.
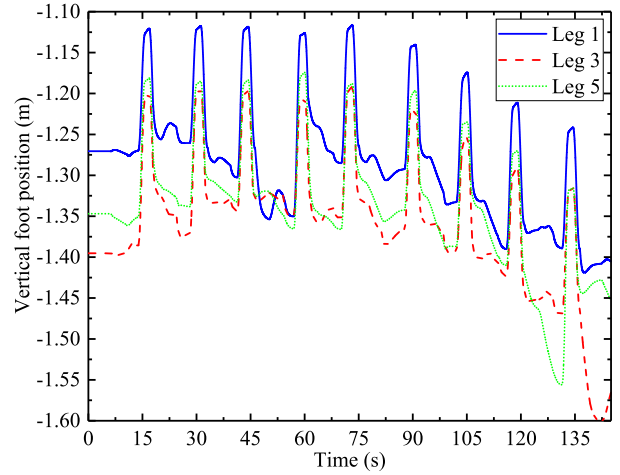

Fig. 20 The vertical foot positions of leg 1, leg 3 and leg 5 with respect to the robot body coordinate C.

Figure 21 shows the vertical foot force comparison of F_{z5} and $F_{z1} + F_{z3}$ during three stance phases. It can be seen that due to the uneven terrain conditions, $F_{z1} + F_{z3} \approx F_{z5}$ is hard to be totally ensured. The deviation between $F_{z1} + F_{z3}$ and F_{z5} leads to the fluctuation of the body's roll angle. But the foot force deviation is

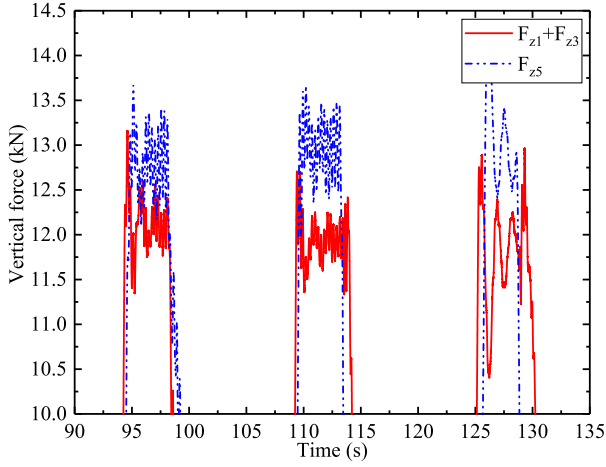acceptable because the roll angle is almost controlled within the stable range.

Fig. 21 The vertical foot force comparison of WEP.

5 Conclusion and future works

In this paper, the importance of the motion stability and the control problems of a large-size hexapod robot have been demonstrated. The main theoretical contribution of this paper is the proposal of a simple control scheme inspired by the biological EPH. The control scheme is mainly based on an EP trajectory modification method which is designed to achieve the system equilibrium of the robot, and deformation counteraction. In this control scheme, no complex dynamics computation is employed. A compliant-leg model which is similar to the muscle-spring model in the EPH has been used and based on this abstracted model, the deformations which will influence the walking stability of the large-size hexapod robot have been significantly considered. Different experiments based on the real large-size hexapod robot have been carried out. The effectiveness of the control scheme in ensuring the walking stability of the robot has been verified through the analyses of the experiment results.

Different from the existing inverse dynamics controllers developed for commonly seen small-size robots, the EP control scheme proposed in this paper shows two significant improvements. The first one is deformation counteraction which is of crucial importance in ensuring the body altitude of the large-size hexapod robot. It can be inferred that with the increase in the mass and payload of a large-size hexapod robot, the advantage of deformation counteraction will become more significant. Furthermore, the deformation counteraction characteristic may allow the robot designers to use low-cost materials to build their robots with larger mechanical errors. The second improvement is the simplicity of the control scheme. The control scheme is totally linear without any nonlinear computations. Regardless of the kinematics differences, the control scheme can be easily employed by other robot designers. Due to the good versatility, more applications of the control scheme on other hexapod robots can be expected.

The EP trajectory modification method proposed in this paper is more like a feed-forward control method. Although the posture fluctuations of the large-size hexapod robot can be reduced to ensure stable locomotion, complete posture tracking can not be realized only using this method. Therefore, to further improve the posture tracking ability, and environment adaptability of the large-size hexapod robot, more trajectory modification methods based on the feedback informations of the sensors will be introduced into the control scheme in the future. Besides, more natural terrain moving experiments will be carried out in the future.

Appendix A

To calibrate the stiffness coefficient of the robot leg, namely K_{iz} in equation (2), a simple method was used.

First, we initialized the robot posture with six legs supporting the robot body on a rigid flat terrain, and set a desired body altitude d. Then we employed a plumb line with one end fixed on the robot body, and the other end perpendicular to the ground. By measuring the length of the plumb line, we obtained the actual body altitude d' under the gravity of the robot. At last, we measured the vertical foot force $^{C}F_{iz}'$ of leg i by reading the feedback data from the 3D contact-force sensor equipped. Based on $^{C}F_{iz}'$ and the body altitude deviation $d-d'$, K_{iz} was obtained, as shown in equation (24). The schematic diagram of the calibration process is shown in Figure 22.

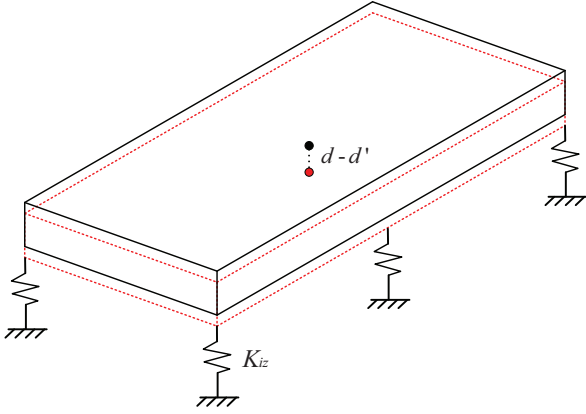$$K_{iz} = \frac{^{C}F_{iz}'}{d - d'} \tag{24}$$

Fig. 22 The schematic diagram of the calibration process.

Appendix B

In the authors' previous work [46], the macro terrain can be nearly abstracted as a support plane which is constructed with all the support feet. The general equation of this plane can be expressed in equation (25), which has the same form as the equation (1) in reference [46].

$$Ax + By + Dz + 1 = 0 \qquad (25)$$

The coefficients of equation (25), namely A, B, and D can be computed using the least square method, as shown in equation (26).

$$\begin{bmatrix} A \\ B \\ D \end{bmatrix} = \begin{bmatrix} a_{11} \ a_{12} \ a_{13} \\ a_{21} \ a_{22} \ a_{23} \\ a_{31} \ a_{32} \ a_{33} \end{bmatrix}^{-1} \begin{bmatrix} -\sum {}^{C}P_{ix}' \\ -\sum {}^{C}P_{iy}' \\ -\sum {}^{C}P_{iz}{}^{*} \end{bmatrix} \qquad (26)$$

with

$$\begin{cases} a_{11} = \sum {}^{C}P_{ix}'^{2} \\ a_{22} = \sum {}^{C}P_{iy}'^{2} \\ a_{33} = \sum {}^{C}P_{iz}{}^{*2} \\ a_{12} = a_{21} = \sum {}^{C}P_{ix}' \cdot {}^{C}P_{iy}' \\ a_{13} = a_{31} = \sum {}^{C}P_{ix}' \cdot {}^{C}P_{iz}{}^{*} \\ a_{23} = a_{32} = \sum {}^{C}P_{iy}' \cdot {}^{C}P_{iz}{}^{*} \\ {}^{C}P_{iz}{}^{*} = {}^{C}P_{iz}' + {}^{C}F_{iz}'/K_{iz} \end{cases} \qquad (27)$$

where ${}^{C}P_{ix}'$, ${}^{C}P_{iy}'$, and ${}^{C}P_{iz}'$ represent the computation-based foot positions of the support leg i along the x, y and z directions in the robot body coordinate C, respectively. ${}^{C}P_{iz}{}^{*}$ represents the actual foot position of the support leg i along the z direction in the robot body coordinate C. ${}^{C}F_{iz}'$ represents the actual vertical foot force of the support leg i achieved from the feedback data of the 3D contact force sensor. K_{iz} represents the vertical stiffness coefficient of the support leg i.

It is well to be noticed that during the computation of equation (26), the three foot positions along different directions are not obtained through the same way. Just as discussed in Section 2.2, the tangential deformation of the support leg i is too small and can be neglected. Therefore, ${}^{C}P_{ix}'$ and ${}^{C}P_{iy}'$ which are obtained through the forward kinematics computation can be used precisely to represent the actual foot positions (the kinematics modeling process of the large-size hexapod robot employed in this paper can be found in the authors' previous work [44]). But for the vertical foot position, because of the obvious vertical deformation of leg i, the forward kinematics computation along the z direction is not accurate enough. In other words, ${}^{C}P_{iz}'$ obtained directly through the forward kinematics computation cannot be used directly to represent the actual foot position. Therefore, ${}^{C}P_{iz}{}^{*}$ with the vertical deformation considered is used to represent the actual vertical foot position.

Based on the A, B, and D computed from equation (26), the perpendicular distance from the origin of the body coordinate C to the support plane, namely the actual body height d' during hexapod locomotion, can be obtained through the computation of equation (28).

$$d' = \frac{1}{\sqrt{A^2 + B^2 + D^2}} \qquad (28)$$

References

1. Semini, C., Barasuol, V., Goldsmith, J., Frigerio, M., Focchi, M., Gao, Y., & Caldwell, D. G. (2016). Design of the hydraulically actuated, torque-controlled quadruped robot HyQ2Max. IEEE/ASME Transactions on Mechatronics, 22(2), 635-646.
2. Gehring, C., Coros, S., Hutler, M., Bellicoso, C. D., Heijnen, H., Diethelm, R., ... & Siegwart, R. (2016). Practice makes perfect: An optimization-based approach to controlling agile motions for a quadruped robot. IEEE Robotics & Automation Magazine, 23(1), 34-43.
3. Li, Z., Zhou, C., Tsagarakis, N., & Caldwell, D. (2016). Compliance control for stabilizing the humanoid on the changing slope based on terrain inclination estimation. Autonomous Robots, 40(6), 955-971.
4. Hodoshima, R., Doi, T., Fukuda, Y., Hirose, S., Okamoto, T., & Mori, J. (2007). Development of a Quadruped Walking Robot TITAN XI for Steep Slope OperationStep Over Gait to Avoid Concrete Frames on Steep Slopes. Journal of Robotics and Mechatronics, 19(1), 13-26.
5. Irawan, A., & Nonami, K. (2011). Compliant walking control for hydraulic driven hexapod robot on rough terrain. Journal of Robotics and Mechatronics, 23(1), 149-162.
6. Zhuang, H. C., Gao, H. B., & Deng, Z. Q. (2017). Gait planning research for an electrically driven large-load-ratio six-legged robot. Applied Sciences, 7(3), 296.
7. Caron, S., Pham, Q. C., & Nakamura, Y. (2016). Zmp support areas for multicontact mobility under frictional constraints. IEEE Transactions on Robotics, 33(1), 67-80.

8. Shadmehr, R., & Mussa-Ivaldi, F. A. (1994). Adaptive representation of dynamics during learning of a motor task. Journal of Neuroscience, 14(5), 3208-3224.

9. Thoroughman, K. A., & Shadmehr, R. (2000). Learning of action through adaptive combination of motor primitives. Nature, 407(6805), 742.

10. Buchanan, T. S., Lloyd, D. G., Manal, K., & Besier, T. F. (2005). Estimation of muscle forces and joint moments using a forward-inverse dynamics model. Medicine and Science in Sports and exercise, 37(11), 1911.

11. Erdemir, A., McLean, S., Herzog, W., & van den Bogert, A. J. (2007). Model-based estimation of muscle forces exerted during movements. Clinical biomechanics, 22(2), 131-154.

12. Russo, M., D'Andola, M., Portone, A., Lacquaniti, F., & d'Avella, A. (2014). Dimensionality of joint torques and muscle patterns for reaching. Frontiers in computational neuroscience, 8, 24.

13. Villard, C., Gorce, P., Fontaine, J. G., & Rabit, J. (1993, October). RALPHY: A dynamic study of a quadruped robot. In Proceedings of IEEE Systems Man and Cybernetics Conference-SMC (Vol. 2, pp. 106-111). IEEE.

14. Li, Z., Ge, Q., Ye, W., & Yuan, P. (2015). Dynamic balance optimization and control of quadruped robot systems with flexible joints. IEEE Transactions on Systems, Man, and Cybernetics: Systems, 46(10), 1338-1351.

15. Roy, S. S., Choudhury, P. S., & Pratihar, D. K. (2010, September). Dynamic modeling of energy efficient hexapod robots locomotion over gradient terrains. In FIRA RoboWorld Congress (pp. 138-145). Springer, Berlin, Heidelberg.

16. Mahapatra, A., Roy, S. S., Bhavanibhatla, K., & Pratihar, D. K. (2015, February). Energy-efficient inverse dynamic model of a Hexapod robot. In 2015 International Conference on Robotics, Automation, Control and Embedded Systems (RACE) (pp. 1-7). IEEE.

17. Hutter, M., Sommer, H., Gehring, C., Hoepflinger, M., Bloesch, M., & Siegwart, R. (2014). Quadrupedal locomotion using hierarchical operational space control. The International Journal of Robotics Research, 33(8), 1047-1062.

18. Wensing, P. M., Kim, S., & Slotine, J. J. E. (2017). Linear matrix inequalities for physically consistent inertial parameter identification: A statistical perspective on the mass distribution. IEEE Robotics and Automation Letters, 3(1), 60-67.

19. Wu, J., Wang, J., & You, Z. (2010). An overview of dynamic parameter identification of robots. Robotics and computer-integrated manufacturing, 26(5), 414-419.

20. Tournois, G., Focchi, M., Del Prete, A., Orsolino, R., Caldwell, D. G., & Semini, C. (2017, September). Online payload identification for quadruped robots. In 2017 IEEE/RSJ International Conference on Intelligent Robots and Systems (IROS) (pp. 4889-4896). IEEE.

21. Abdellatif, H., & Heimann, B. (2009). Advanced model-based control of a 6-DOF hexapod robot: A case study. IEEE/ASME Transactions On Mechatronics, 15(2), 269-279.

22. Grotjahn, M., Heimann, B., & Abdellatif, H. (2004). Identification of friction and rigid-body dynamics of parallel kinematic structures for model-based control. Multibody System Dynamics, 11(3), 273-294.

23. Wang, P., Zheng, P., Zha, F., & Dong, Y. (2018, July). Force Control Method for Pantograph Leg of Large-scale Heavy-duty Legged Robot. In 2018 3rd International Conference on Advanced Robotics and Mechatronics (ICARM) (pp. 24-29). IEEE.

24. Ding, L., Gao, H., Deng, Z., Song, J., Liu, Y., Liu, G., & Iagnemma, K. (2013). Footterrain interaction mechanics for legged robots: Modeling and experimental validation. The International Journal of Robotics Research, 32(13), 1585-1606.

25. Feldman, A. G. (1966). Functional tuning of the nervous system with control of movement or maintenance of a steady posture-II. Controllable parameters of the muscle. Biofizika, 11, 565-578.

26. Feldman, A. G. (2009). Origin and advances of the equilibrium-point hypothesis. In Progress in motor control (pp. 637-643). Springer, Boston, MA.

27. Asratyan, D. G., & Feldman, A. G. (1965). Functional tuning of the nervous system with control of movement or maintenance of a steady posture. 1. Mechanographic analysis of the work of the joint on execution of a postural task. Biphysics, 10, 925.

28. Bizzi, E., Mussa-Ivaldi, F. A., & Giszter, S. (1991). Computations underlying the execution of movement: a biological perspective. Science, 253(5017), 287-291.

29. Shadmehr, R., & Arbib, M. A. (1992). A mathematical analysis of the force-stiffness characteristics of muscles in control of a single joint system. Biological cybernetics, 66(6), 463-477.

30. Suzuki, M., & Yamazaki, Y. (2005). Velocity-based planning of rapid elbow movements expands the control scheme of the equilibrium point hypothesis. Journal of computational neuroscience, 18(2), 131-149.

31. Latash, M. L. (2010). Stages in learning motor synergies: A view based on the equilibrium-point hypothesis. Human movement science, 29(5), 642-654.

32. Ambike, S., Mattos, D., Zatsiorsky, V. M.,& Latash, M. L. (2016). Synergies in the space of control variables within the equilibrium-point hypothesis. Neuroscience, 315, 150-161.

33. Gomi, H., & Kawato, M. (1996). Equilibrium-point control hypothesis examined by measured arm stiffness during multijoint movement. Science, 272(5258), 117-120.

34. Popescu, F. C., & Rymer, W. Z. (2000). End points of planar reaching movements are disrupted by small force pulses: an evaluation of the hypothesis of equifinality. Journal of Neurophysiology, 84(5), 2670-2679.

35. Hinder, M. R., & Milner, T. E. (2003). The case for an internal dynamics model versus equilibrium point control in human movement. The Journal of Physiology, 549(3), 953-963.

36. Gu, X., & Ballard, D. H. (2006, June). Robot movement planning and control based on equilibrium point hypothesis. In 2006 IEEE Conference on Robotics, Automation and Mechatronics (pp. 1-6). IEEE.

37. Mukaibo, Y., Park, S., & Maeno, T. (2004). Equilibrium point control of a robot arm with a double actuator joint. International Simposium on Robotics and Automation.

38. Kim, B. S., Park, S., Song, J. B., & Kim, B. (2013). Equilibrium point control of a robot manipulator using biologically-inspired redundant actuation system. Advanced Robotics, 27(8), 567-579.

39. Park, S., Lim, H., Kim, B. S., & Song, J. B. (2006, October). Development of safe mechanism for surgical robots using equilibrium point control method. In International Conference on Medical Image Computing and Computer-Assisted Intervention (pp. 570-577). Springer, Berlin, Heidelberg.

40. Jain, A., & Kemp, C. C. (2009, December). Pulling open novel doors and drawers with equilibrium point control. In 2009 9th IEEE-RAS International Conference on Humanoid Robots (pp. 498-505). IEEE.

41. Geng, T., & Gan, J. Q. (2009). Planar biped walking with an equilibrium point controller and state machines. IEEE/ASME Transactions on Mechatronics, 15(2), 253-260.

42. Shi, Y., Wang, P., Wang, X., Zha, F., Jiang, Z., Guo, W., & Li, M. (2018). Bio-inspired equilibrium point control scheme for quadrupedal locomotion. IEEE Transactions on Cognitive and Developmental Systems.

43. Metta, G., Panerai, F., Manzotti, R., & Sandini, G. (2000, September). Babybot: an artificial developing robotic agent. In Proc. Sixth Int. Conf. on the Simulation of Adaptive Behaviors (SAB 2000), Paris, France.

44. Chen, C., Guo, W., Zheng, P., Zha, F., Wang, X., & Jiang, Z. (2019). Stable Motion Control Scheme Based on Foot-Force Distribution for a Large-Scale Hexapod Robot. In 2019 IEEE 4th International Conference on Advanced Robotics and Mechatronics (pp. 763-768), Toyonaka, Japan.

45. Gardner, J. F., Srinivasan, K., & Waldron, K. J. (1990). A solution for the force distribution problem in redundantly actuated closed kinematic chains. Journal of Dynamic Systems, Measurement, and Control, 112(3), 523-526.

46. Zha, F., Chen, C., Guo, W., Zheng, P., & Shi, J. (2019). A free gait controller designed for a heavy load hexapod robot. Advances in Mechanical Engineering, 11(3), 1687814019838369.

47. Irawan, A., & Nonami, K. (2011). Optimal impedance control based on body inertia for a hydraulically driven hexapod robot walking on uneven and extremely soft terrain. Journal of Field Robotics, 28(5), 690-713.

48. Wang, G., Ding, L., Gao, H., Deng, Z., Liu, Z., & Yu, H. (2020). Minimizing the Energy Consumption for a Hexapod Robot Based on Optimal Force Distribution. IEEE Access, 8, 5393-5406.

49. Wang, P., Zheng, P., Zha, F., & Dong, Y. (2018). Force Control Method for Pantograph Leg of Large-scale Heavy-duty Legged Robot. In 2018 IEEE International Conference on Advanced Robotics and Mechatronics (pp. 24-29).